Why the pyrochlore-like antiferromagnet NaCu3F7 is magnetically non-frustrated

Julien Lévêque, Elisa Rebolini, Marie-Bernadette Lepetit, Andrés Saúl

Why the pyrochlore-like antiferromagnet $NaCu_3F_7$ is magnetically non-frustrated

Julien Lévêque,[1,2] Elisa Rebolini,[3] Marie-Bernadette Lepetit,[4,3,*] and Andrés Saúl[1,†]

[1] *Aix Marseille Univ, CNRS, CINAM, Marseille, France*
[2] *Univ. Grenoble Alpes, CNRS, Grenoble INP, Institut Néel, Grenoble, France*
[3] *Institut Laue Langevin, Grenoble, France*
[4] *Institut Néel, CNRS, Grenoble, France*

We present a theoretical study of the magnetic properties for the highly geometrically-frustrated $NaCu_3F_7$ compound, surprisingly experimentally presenting little or no frustration. The magnetic effective exchange interactions were calculated using explicitely correlated *ab-initio* methods. A model Hamiltonian was built from these interactions and used to determine the zero temperature magnetic order versus magnetic field, using a quantum Heisenberg Hamiltonian or, for comparison, a spin 1/2 Ising Hamiltonian. The magnetic order at zero magnetic field is non frustrated and associated with to the propagation vector $\vec{q} = (0, 0, 0)$. The magnetization versus magnetic field reveals the existence of a 1/3 plateau that could be observed in high-pulsed magnetic field experiments. Analysing the magnetic interactions, we highlight the importance of the magnetic ion nature and the lattice distortion in the non-frustrated nature of the $NaCu_3F_7$ magnetic structure, despite its triangular/Kagome subnetworks. We believe that this non-frustrated behaviour could also take place in other triangular copper-based systems.

I. INTRODUCTION

Studying the binary diagram of $NaF - CuF_2$, Renaudin et al. discovered a new compound $NaCu_3F_7$ [1]. $NaCu_3F_7$ was the first example of copper fluorides with copper ions in two different coordination polyhedra, namely octahedra and square planar coordination. This compound is closely related to the weberite structural family ($A_2B_2X_7$) that attracted a lot of attention due to its highly frustrated geometry [2]. Related to the pyrochlore structure, the weberites exhibit a wide range of properties such as magnetic, dielectric or photo-catalytic ones [2–5], making them interesting for both chemical processes [6–8] and electronic applications [9]. The weberite structure forms stacked Kagome networks by alternatively using the A/B atoms to form the hexagons, whose centres are occupied by B/A atoms [2].

In the specific case of $NaCu_3F_7$, half of the A atoms are replaced by copper (i.e. identical to the B atoms). At room temperature, $NaCu_3F_7$ has a centred monoclinic structure, space group $C2/c$ [1]. All the sodium atoms are equivalent by symmetry, but there are three non-equivalent copper atoms (see Fig. 1) and four non-equivalent F atoms. Two copper atoms (Cu1 and Cu2) are located in CuF_6 corner-sharing elongated octahedra and the third one (Cu3) is in a CuF_4 corner-sharing square. Along the $\vec{c}$ direction, the Cu1 F_6 octahedra form chains, while the Cu2 F_6 ones and the Cu3 F_4 squares alternate to form the neighbouring chains. The Cu1 and Cu2-Cu3 chains share fluorine atoms and form (110) and $(\bar{1}10)$ planes, intersecting at an angle of 62.41° on a Cu1 chain along the $\vec{c}$ axis (see Fig 1).

Formal charge analysis shows that the magnetism is supported by the Cu^{2+} ions, that form a distorted Kagome network in the $(\vec{a}, \vec{b})$ plane (see Fig. 1 or Fig. 2 a). The hexagon centres are occupied by the sodium atoms and the Kagome networks stacked along the $\vec{c}$ direction. In addition to the Kagome planes, the copper atoms form

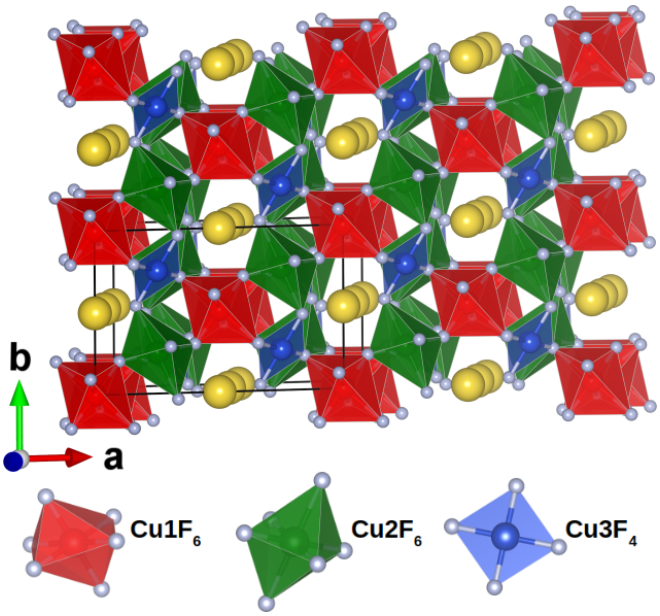

Figure 1. Schematic representation of the $NaCu_3F_7$ crystal structure. The F atoms are in light gray, and the Na in yellow. The three independent Cu are pictured in different colours : Cu1 in red, Cu2 in green and Cu3 in blue.

distorted triangular lattices (see Fig. 2 b) along the (110) and $(1\bar{1}0)$ directions. The nearest-neighbour Cu-Cu distances are all between 3.46 and 3.73 Å.

This highly frustrated geometry, lead Renaudin *et al.* in 1988 [1] to predict magnetic frustration in the $NaCu_3F_7$ system. Two years latter, an abnormally high magnetic ordering temperature, $T_N = 71$ K, was ob-

* Marie-Bernadette.Lepetit@neel.cnrs.fr
† andres.saul@cnrs.fr

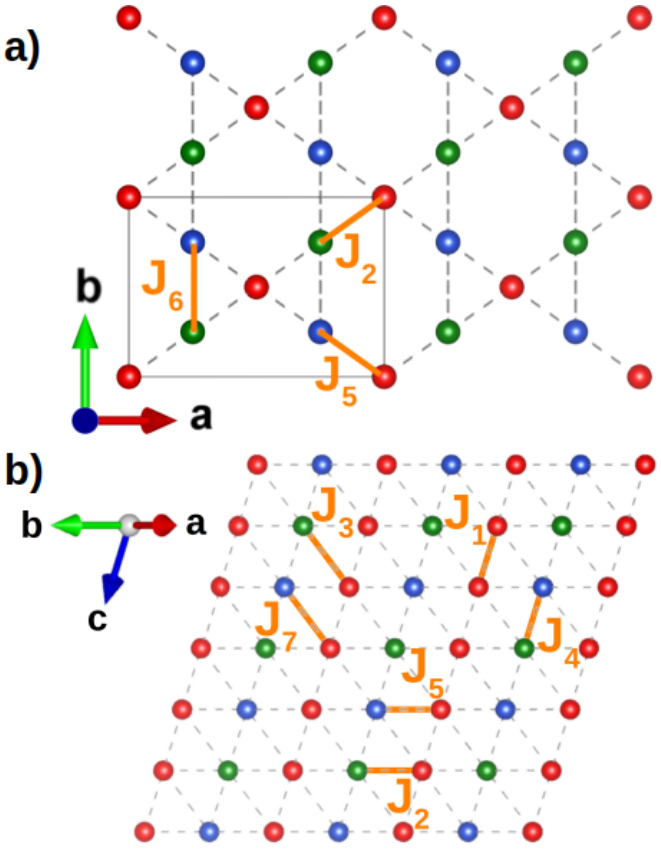

Figure 2. Schematic representation of the frustrated Kagome (001) and triangular (110) copper networks in $NaCu_3F_7$ a) along the $\vec{c}$ direction and b) in the (110) plane. Naming of the magnetic interactions are added. The Cu atoms are represented in red Cu1, green Cu2 or blue Cu3.

tained from magnetic susceptibility measurements by the same group [10], casting doubts on the existence of a magnetic frustration. Neutron diffraction experiments have then been performed and the proposed magnetic structure was also compatible with the absence of frustration, eventhough the small number of available reflections prevented the authors to draw direct conclusions. Other arguments can be suggested to support the absence of magnetic frustration. First, the ordering temperature is unusually high for cupric fluorides, and more specifically for copper-based weberites, as the latter hardly exhibit a 3D magnetic ordering at a temperature higher than a few kelvins [11]. Secondly, the Curie-Weiss temperature of $\Theta_{CW} = -184$ K gives a frustration parameter [12] $f = -\Theta_{CW}/T_N \approx 3$ below the values ($f > 10$) that Ramirez [12] suggests as defining materials with strong geometrical frustration.

It remains to understand the reasons for the absence of magnetic frustration despite the presence of a Kagome and a triangular lattice. In their 1990 paper, Renaudin *et al* [10] suggested that the nature and orientation of the Cu^{2+} magnetic orbitals could be at hand. They proposed a guess on the nature of the magnetic orbitals involved in each magnetic interaction and predicted its character (ferromagnetic or antiferromagnetic). To our knowledge, no additional studies have been published to either corroborate or challenge these hypotheses, nor to provide further clarity on the magnetic behaviour.

The aim of this paper is thus to study the effective magnetic interactions and the resulting magnetic ordering in the $NaCu_3F_7$ compound, in order to provide a theoretical explanation of non-frustrated magnetic behaviour as hinted at by experimental observations and to ground the amplitude and sign of the magnetic interactions in the geometry and electronic structure.

II. TECHNICAL DETAILS

The methodology used in this work is similar the the one used in some of our previous works such as Ref. [13]. Nevertheless for a better understanding we detailled it in this section.

A. *Ab*-initio calculations

In order to correctly describe the exchange-correlation effects which are responsible for the magnetic interactions, those will be computed using a multireference configuration interaction method, namely the complete active space plus single and double excitations from the difference dedicated configuration interaction space (CAS+DDCI) method [14]. As such configuration interaction methods require the diagonalization of large matrices, they can only be applied to formally finite-size systems. We have therefore designed, for each magnetic integral, appropriate fragments embedded in a set of renormalized charges [15] and total ions pseudo-potentials (TIPS) [16], in order to reproduce the effects of the rest of the crystal on the quantum fragment. The TIPS reproduce the exclusion effects due to the electrons of the first layers surrounding the fragment, and the set of charges is chosen in order to reproduce the Madelung potential seen by the fragment with an error of less than 0.1 meV. The quantum fragments were chosen so that to include the magnetic atoms associated with the desired interaction, their first coordination shell, and any additional bridging ligands.

The fragment orbitals were optimized within a complete active space self consistent field [17] (CASSCF) calculation on the 3d open-shell electrons of the Cu^{2+} ions, using the MOLCAS package [18]. We used a valence basis set of $3\zeta + P$ quality, associated to the relativistic core pseudo-potentials of the Stuttgart group [19]. The CAS+DDCI calculations were then performed using the RelaxSE code [20]. The latter provides the fragment low-energy excitations, from which the effective exchange integrals can be deduced.

The crystal structure used in all calculations is the room temperature X-Ray structure given in Ref. [1].

B. Exact diagonalization

The magnetisation versus magnetic field has been evaluated using a Lanczos diagonalization of the Heisenberg Hamiltonian derived from our *ab-initio* calculations. The calculations were done on a finite lattice of 24 spins with periodic boundary conditions.

While the matrix exhibits a block diagonal structure with a sector of Sz, the blocks associated with smaller Sz values prove challenging for complete diagonalization due to their substantial size. To address this, an extensive calculation of at least 1000 lower-energy states has been undertaken for each sector. This approach ensures accurate treatment of the ground state and the consideration of temperature effects for low temperature values.

C. Monte-Carlo calculations

The Monte Carlo (MC) simulations were performed on the same Heisenberg Hamiltonian mentioned above. For this purpose we used the standard Metropolis algorithm [21] on a classical approximation of the spin Hamiltonian. The phase space sampling was done using an adaptive algorithm, keeping the acceptance rate close to 50%, as proposed by Alzate-Cardona et al. [22]. To prevent numerical catastrophic cancellation while computing the specific heat, we used the Welford algorithm [23]. At each temperature, 500 Monte-Carlo steps per atom (MCS) were performed, to ensure the thermal equilibrium and a good approximation of the mean magnetic energy. The specific heat was then computed using a thermodynamical average performed with 10 000 MCS. The calculations were performed using supercells up to $20a \times 20b \times 20c$ (96000 magnetic atoms).

III. RESULTS AND DISCUSSION

A. Magnetic integrals

The formal charge analysis of $NaCu_3F_7$ yields $Na^+Cu^{2+}F_3^-$ corresponding to a $3d^9$ Copper electronic configuration. The corresponding theoretical magnetic moments are $S_{\mathrm{Cu}} = 1/2$, which is fully consistent with the magnetic moments found in powder neutron scattering [10].

The magnetic exchange interactions were obtained from the *ab-initio* calculations, by mapping the computed magnetic spectra onto the energy spectra of a Heisenberg Hamiltonian on the same fragments

$$\hat{H}_{\mathrm{Heis}} = -\sum_{<i,j>} J_{ij} \left(\hat{\mathbf{S}}_i \cdot \hat{\mathbf{S}}_j - \frac{\hat{n}_i \hat{n}_j}{4} \right) \qquad (1)$$

where $\hat{\mathbf{S}}_i$ and $\hat{\mathbf{S}}_j$ are the quantum spin operators associated with the first-neighbour i and j sites; J_{ij} are the effective exchange interactions, positive and negative values corresponding to ferromagnetic (FM) and antiferromagnetic (AFM) interactions.

We computed seven independent interactions (see Fig. 2) that are reported in Table I. One can see that the three dominant interactions, namely J_1, J_2 and J_4, are AFM, unlike what was guessed by Renaudin *et al.* [10] that supposed J_4 to be FM. These interactions are much larger than the others, and will dominate the magnetic behaviour of the compound. Indeed, the remaining interactions are FM and very weak.

Table I. Effective exchange interactions obtained from ab-initio calculations. The associated metal-metal distances d_{M-M}, superexchange path and metal-ligand-metal angles are also reported. Negative values correspond to AFM interactions and positive to FM ones.

J_i	Value [meV]	d_{M-M} [Å]	Superexchange paths	Angle [°]
J_1	-12.33	3.462	Cu1-F4-Cu1	131.2
J_2	-20.13	3.544	Cu1-F1-Cu2	138.7
J_3	0.28	3.723	Cu1-F2-Cu2	121.5
J_4	-8.10	3.462	Cu2-F2-Cu3	124.9
J_5	0.24	3.544	Cu1-F2-Cu3	111.3
J_6	0.50	3.672	Cu2-F3-Cu3	123.7
J_7	0.01	3.723	-	-

Let us now analyse the physical effects at work in magnetic interactions in order to better understand these results. It is well known [24, 25] that effective magnetic exchange integrals can be understood within the quasi-degenerate perturbation theory formalism [26] at the fourth order. It comes as

$$J \simeq \underbrace{2K}_{J^{(1)}} \underbrace{-4\frac{t_{MM}^2}{U_M}}_{J^{(2)}} \underbrace{-4\frac{t_{LM}^4}{U_M \Delta^2} - 8\frac{t_{LM}^4}{(2\Delta + U_L)\Delta^2}}_{J^{(4)}} \qquad (2)$$

where K is the Pauli direct exchange integral (always FM), t_{MM} the transfer integral between the two magnetic orbitals, and U_M its energetic cost, t_{LM} is the bridging-ligand to metal transfer integral and Δ its energetic cost.

The $J^{(1)}$ first-order contribution essentially depends on the metal-metal distance and the magnetic orbitals orientation. Indeed, if m_1 and m_2 stands for the magnetic orbitals on the two copper sites, at first order expansion in the Cu-Cu distance, R, one gets $J^{(1)} \simeq 2\langle m_1 | m_2 \rangle^2 / R$. The $J^{(2)}$ second-order contribution depends as well on the metal-metal distance and the magnetic orbitals orientation, except that the magnetic orbitals overlap is replaced by the hopping integral between the latter. The fourth-order contribution, $J^{(4)}$, mostly depends on the overlap between the metal magnetic orbitals and the bridging-ligand orbitals. As a conclusion, not only the magnetic exchange integral depends on the metal-metal distance but also on the metal-ligand ones and more importantly on the nature and relative orientation of the

magnetic orbitals. This analysis implicitly supports the Kanamori-Goodenough rules [27]).

In $NaCu_3F_7$ the copper magnetic orbitals are all of $d_{x^2-y^2}$ nature, pointing toward the F atoms in the squares pictured in Fig 3. In order to better understand the amplitude of the magnetic interactions, let us analyse the difference between the J_2 and J_5 interactions that do correspond to equivalent metal-metal distances, but very different magnetic exchanges. Picturing their magnetic and bridging-ligand orbitals (see Fig. 4), one sees immediately that while both magnetic orbitals in the J_2 interaction are approximately pointing toward each-other and toward the bridging F atom, in the J_5 interaction only the Cu3 orbital is pointing toward the bridging F atom, the Cu1 magnetic orbital being nearly parallel (but in another plane) to the Cu3 one. As a result, not only no orbital of the bridging F atom can participate in the $J^{(4)}$ super-exchange term, but also the overlap between the two magnetic orbitals is very small. As a result, all terms in J_5 are nearly zero. The magnetic orbitals involved in the J_3, J_6 and J_7 interactions present similar orientations, thus resulting in nearly nil magnetic exchange integrals.

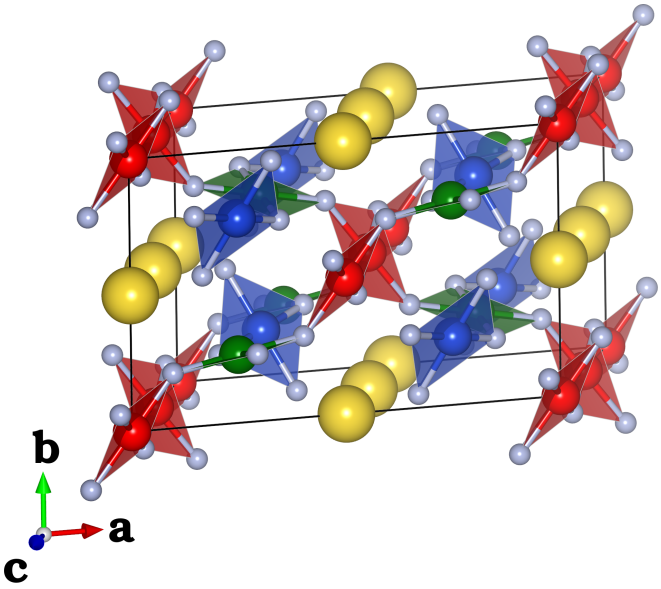

Figure 3. Schematic picture of the squares supporting the $d_{x^2-y^2}$ magnetic orbitals in $NaCu_3F_7$. The $d_{x^2-y^2}$ point toward the F atoms (in gray) at the square corners.

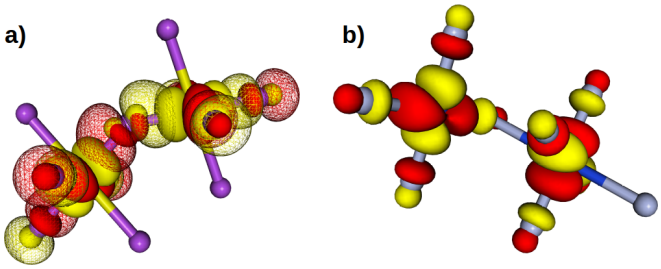

Figure 4. Computed magnetic and bridging-ligand orbitals in the a) J_2 and b) J_5 magnetic interactions. The magnetic orbitals are drawn using solid isodensity curves, while the bridging-ligand orbital is drawn using wireframe isodensity curves.

As implicit in Fig. 3, and well-known from the ligand-field theory, the Cu magnetic orbitals point toward the closest F ligands. Table II reports the coppers-to-bridging-ligand distances for the seven magnetic interactions. One sees immediately that the nil interactions are directly related with the existence of a metal to bridging-ligand distance larger than the typical Cu-F distance (~ 1.9Å). Indeed, such a distance not only means that the magnetic orbital of that copper is not pointing toward the ligand, but also that it has a weak overlap with the other copper magnetic orbital. As we will see in the next section, those large differences in the magnetic interactions for similar copper-copper distances will induce a magnetic network different from the Kagome and triangular one pictured in Fig 2.

Table II. Metals-to-bridging-ligand distances (in Å) and decomposition of the exchange integrals in the direct and super-exchange terms (in meV).

J_i	d_{M_1-L}	d_{M_2-L}	$J^{(1)}$	$J^{(2)}+J^{(4)}$
J_1	1.901	1.901	2.024	−14.350
J_2	1.906	1.891	2.569	−22.694
J_3	2.322	1.940	0.069	0.209
J_4	1.940	1.964	1.469	−9.573
J_5	3.322	1.964	0.060	0.184
J_6	2.297	1.861	0.111	0.387
J_7	-	-	0.010	0.005

B. Magnetic order at zero temperature

The magnetic order in the ground state can be easily deduced from the above main three interactions.

The leading interaction J_2 orders AFM spin chains in the $\vec{a}+\vec{b}$ direction. When adding J_1 a 3D, non-frustrated, AFM order is created in the (110) and ($\bar{1}$10) planes. This order involves the Cu1 and Cu2 atoms. The third leading interaction, J_4, integrates the Cu3 atoms into this order without adding any frustration. The FM interactions, J_3, J_6, and J_7, are also consistent with this magnetic order, whereas the remaining interaction, J_5, will bring some frustration but so weak it can be considered negligible. Indeed, assuming a classical Ising Hamiltonian the magnetic energy associated with J_5 is $8\,J_5\,S^2 = 0.5$ meV per unit cell (12 Cu atoms), that is less than 1% of the magnetic energy due to the others interactions $[4\,J_1+8\,(J_2+J_4)-8\,(J_3+J_6+J_7)]\,S^2 = -70.3$ meV. One should note that this weak energetic contribution of the J_5 interaction is in agreement with the weak value of the frustration parameter [12] f =

$-\Theta_{CW}/T_N \approx 3$ as can be deduced from the Curie-Weiss temperature.

One can thus safely predict a 3D, non-frustrated AFM order (pictured in Fig.5), associated with a propagation vector $\vec{q} = (0, 0, 0)$ (in good agreement with Ref [10]).

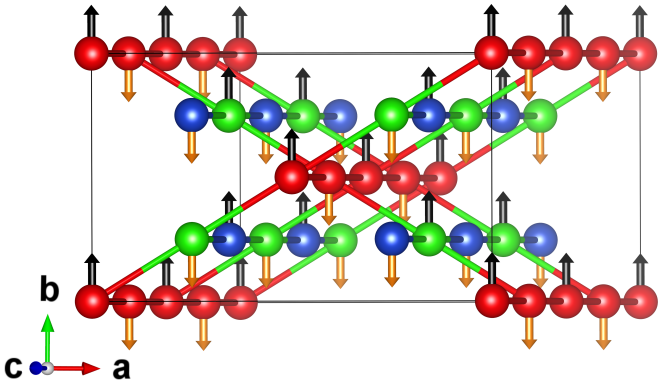

Figure 5. Ground-state magnetic order. The global spin orientation is arbitrary. The three independent Cu are pictured in different colors : Cu1 in red, Cu2 in green and Cu3 in blue. The red-red lines represent the J_1 magnetic interactions, the red-green lines represent J_2, and the green-blue lines represent J_4.

C. Magnetic order with temperature and field

The total magnetization versus magnetic field is obtained at zero temperature from the Lanczos diagonalization of the quantum Heisenberg Hamiltonian. It is shown in Fig. 6.a. The magnetization goes from 0 to 1 with two main plateaus at 1/3 and 2/3. The finite size of the unit cell (24 spins) is responsible for the presence of the other $j/12$ plateaus ($j = 0, \ldots, 12$) which are therefore to be considered as simulation artefacts.

The mean values of the nearest-neighbour spin-spin correlations, $< \hat{\mathbf{S}}_i \cdot \hat{\mathbf{S}}_j >$, associated with the three leading interactions (J_2, J_1, and J_4) are shown in Fig. 6.b). At zero magnetic field the three correlations are negative (respectively -0.402, -0.248, and -0.304) in agreement with the AFM character of the magnetic order.

The Cu3 magnetization (blue line in Fig. 6a)) clearly shows that the 1/3 plateau corresponds to the ordering of the Cu3 moments along the magnetic field. Simultaneously the Cu2 magnetization (green line in Fig. 6a)) orders opposite to the field, in order to keep the magnetic energy minimum. Indeed, the only important interaction involving Cu3 is J_4 that couples it antiferromagnetically to the Cu2 atoms. The 2/3 plateau is not characterised by the full ordering of another copper atom along the field, but rather by the partial contribution of the Cu1 and Cu2 magnetic moments. The contribution of the Cu2 ion is reflected by the J_4 exchange interaction, as can be seen by the positive value of the spin-spin correlation associated to it. This correlation is about 0.11 to be compared with 0.25 corresponding to a full FM order. Eventhough we believe that this plateau will remain for an infinity system, its confirmation would require calculations that are currently unfeasible with the numerical techniques used in this work.

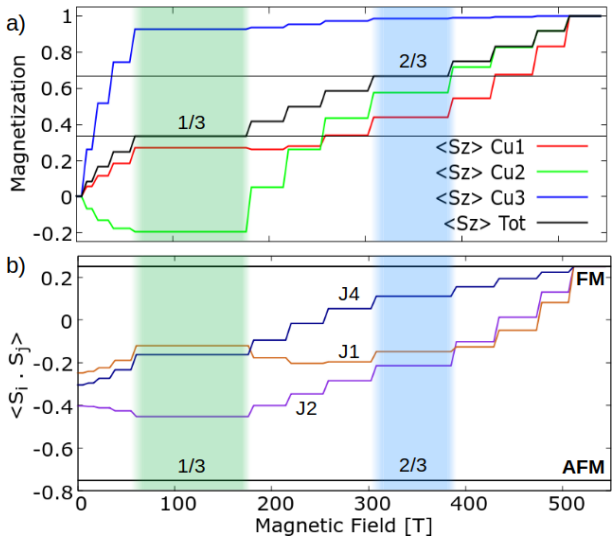

Figure 6. Magnetic moments (a) and spin-spin nearest-neighbour correlations (b) at $T = 0$ K, versus magnetic field, obtained from the diagonalisation of the quantum Heisenberg Hamiltonian using a double unit cell containing 24 spins. a) The red, green and blue curves represent the average magnetic moments of the Cu1, Cu2, and Cu3 atoms respectively while the average total magnetization is in black. b) $< \hat{\mathbf{S}}_i \cdot \hat{\mathbf{S}}_j >$ associated with J_4 (blue), J_1 (brown), and J_2 (magenta).

The magnetization versus magnetic field is shown in Fig. 7 at 0 K, 5 K and 10 K. The calculations were performed using either a classical Ising or a quantum Heisenberg Hamiltonian, with the exchange interactions given in Table I. The two Hamiltonians qualitatively show a similar physical picture, with the existence of 1/3 and 2/3 plateaus when the magnetic field is increased. It's worth highlighting that the classical Hamiltonian can be successfully solved analytically for a cell containing 24 spins. Additionally, this result is further corroborated by observations using a Monte Carlo method for systems up to 96000 spins.

The specific heat versus temperature was computed using the classical Ising Hamiltonian to estimate the Néel temperature at zero magnetic field. The MC average energy at low temperature is about -69.8 meV per unit cell, in good agreement with the theoretical ground-state energy of the predicted magnetic order ($-70.3 + 0.5 = -69.8$ meV). The specific heat shows a transition temperature near 100 K (see Fig. 8) to be compared to the experimental transition temperature at 71 K [10].

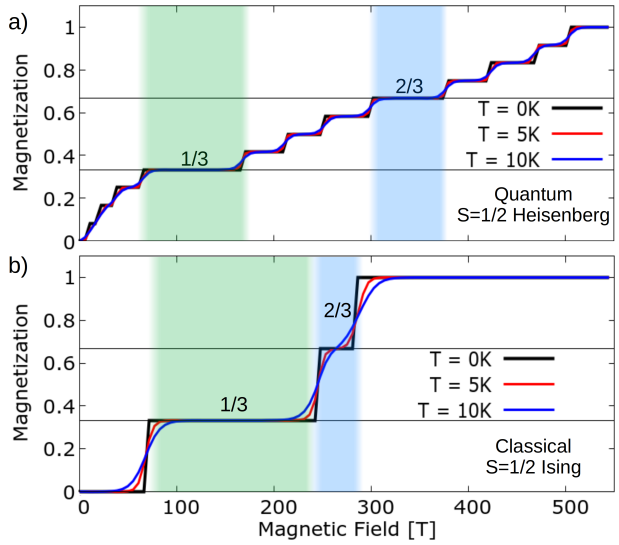

Figure 7. Magnetization versus magnetic field at 0 K (black), 5 K (red) and 10 K (blue). a) Quantum $S = 1/2$ Heisenberg Hamiltonian and b) classical $S = 1/2$ Ising Hamiltonian. In both calculations, a double unit cell containing 24 spins have been used.

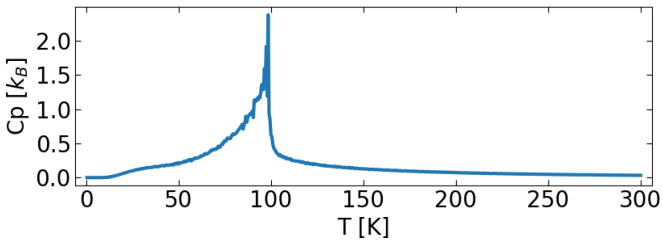

Figure 8. Monte Carlo specific heat versus temperature calculated with a classical Ising Hamiltonian.

IV. CONCLUSION

We carried out a complete magnetic and thermodynamic analysis of the $NaCu_3F_7$ compound, determining the effective low energy magnetic Hamiltonian and its properties.

Despite the fact that $NaCu_3F_7$ appears as a highly geometrically-frustrated compound, the experimental data exhibit a non-frustrated magnetic behaviour. Our evaluation of the effective magnetic integrals was able to explain this apparent contradiction and theoretically confirm the non frustrated behaviour of the $NaCu_3F_7$. Indeed, due to the strong distortions of the CuO_6 octahedra, the orientation of the copper magnetic orbitals is such that there are only three non-negligible magnetic interactions, irrespective of the metal-metal distances. These interactions result in a very-stable, AFM, non-frustrated ground-state at $\vec{q} = (0, 0, 0)$.

We studied the magnetic ordering temperature using Monte-Carlo simulations (Ising model), and found a ordering transition close to 100 K, i.e. of the same order of magnitude as the experimental one.

We then studied the evolution of the magnetic structure under magnetic field and exhibited the existence of a 1/3 and probably a 2/3 magnetization plateaus under the applied field. The 1/3 plateau was shown to be associated with the alignment along the field of the Cu3 atoms, which spin reversal is associated with the lowest magnetic energy. The 2/3 plateau is not associated with the alignment of another type of copper atoms, but shows partial contributions of both the Cu1 and Cu2 atoms. MC simulations show that these plateaus also exist at non-zero temperature ; the 1/3 one being located around 100 T, it could possibly be observed during pulsed high-field experiments.

Finally, let us point out that the unique magnetic orbital of the Cu^{2+} ions allows strong AFM interactions in only two directions, the two directions with the closest ligands. As a result, small geometrical distortions, such as a small increase of the Cu-Ligand distances in one direction and a decrease in another, can modify the orientation of the magnetic orbital. Consequently, they can switch off the magnetic interactions along one direction and switch it on along the other. Such large effects to small distortions are thus the perfect tools to lower the energy in geometrically frustrated systems, and prevent the magnetic frustration that should have resulted from the geometric one.

ACKNOWLEDGMENTS

We acknowledge financial support from the ANR HTHPCM. This work was performed using computer resources obtained from GENCI-IDRIS and CRIANN under projects N°91842 and N°2007013.

The figures 1, 2, 3, 5 were drawn using VESTA [28] and figure 4 using MOLEKEL [29].

[1] J. Renaudin, A. D. Kozak, M. Samouel, M. leblanc, and G. Ferey, Journal of Solid State Chemistry **73**, 603 (1988).
[2] L. Cai and J. C. Nino, Acta Crystallographica Section B Structural Science **65**, 269 (2009).
[3] A. Boireau, P. Gravereau, J. M. Dance, A. Tressaud, and P. Hagenmuller, Mat. Res. Bull. **28**, 27 (1992).
[4] L. Cai and J. C. Nino, Journal of the European Ceramic Society **27**, 3971 (2007).
[5] R. Abe, M. Higashi, Z. Zou, K. Sayama, Y. Abe, and H. Arakawa, The Journal of Physical Chemistry B **108**, 811 (2004).
[6] N. Preux, A. Rolle, C. Merlin, M. Benamira, M. Malys, C. Estournes, A. Rubbens, and R.-N. Vannier, Comptes

Rendus Chimie **13**, 1351 (2010).
[7] F. Wu, P. Wu, L. Chen, and J. Feng, Journal of the European Ceramic Society **39**, 2210 (2019).
[8] H. Euchner, O. Clemens, and M. A. Reddy, npj Computational Materials **5**, 31 (2019).
[9] I. M. Gussev, E. C. O'Quinn, M. Tucker, R. C. Ewing, C. Overstreet, J. Neuefeind, M. Everett, Q. Zhang, D. Sprouster, D. Olds, G. Baldinozzi, and M. Lang, Journal of Materials Chemistry A **11**, 8886 (2023).
[10] J. Renaudin, G. Ferey, A. de Kozak, and M. Samouël, Journal of Magnetism and Magnetic Materials **87**, 57 (1990).
[11] N. Ruchaud, J. Grannec, P. Gravereau, P. Nunez, A. Tressaud, W. Massa, G. Frenzen, and D. Babel, Zeitschrift für anorganische und allgemeine Chemie **610**, 67 (1992).
[12] A. P. Ramirez, Annual Review of Materials Science **24**, 453 (1994).
[13] J. Lévèque, E. Rebolini, M.-B. Lepetit, and A. Saul, Phys. Rev. B **106**, 224402 (2022).
[14] J. Miralles, O. Castell, R. Caballol, and J.-P. Malrieu, Chemical Physics **172**, 33 (1993).
[15] A. Gellé and M.-B. Lepetit, J. Chem. Phys. **128**, 244716 (2008).
[16] N. W. Winter, R. M. Pitzer, and D. K. Temple, J. Chem. Phys. **86**, 3549 (1987).
[17] B. O. Roos, P. R. Taylor, and P. E. Sigbahn, Chem. Phys. **48**, 157 (1980).
[18] F. Aquilante, J. Autschbach, R. K. Carlson, L. F. Chibotaru, M. G. Delcey, L. De Vico, I. Fdez. Galván, N. Ferré, L. M. Frutos, L. Gagliardi, M. Garavelli, A. Giussani, C. E. Hoyer, G. Li Manni, H. Lischka, D. Ma, P. A. Malmqvist, T. Müller, A. Nenov, M. Olivucci, T. B. Pedersen, D. Peng, F. Plasser, B. Pritchard, M. Reiher, I. Rivalta, I. Schapiro, J. Segarra-Martí, M. Stenrup, D. G. Truhlar, L. Ungur, A. Valentini, S. Vancoillie, V. Veryazov, V. P. Vysotskiy, O. Weingart, F. Zapata, and R. Lindh, J. Comp. Chem. **37**, 506 (2016).
[19] M. Dolg, U. Wedig, H. Stoll, and H. Preuss, J. Chem. Phys. **86**, 866 (1987).
[20] E. Rebolini and M.-B. Lepetit, J. Chem. Phys. **154**, 164116 (2021).
[21] N. Metropolis, A. W. Rosenbluth, M. N. Rosenbluth, A. H. Teller, and E. Teller, J. Chem. Phys. **21**, 1087 (1953).
[22] J. D. Alzate-Cardona, D. Sabogal-Suárez, R. F. L. Evans, and E. Restrepo-Parra, Journal of Physics: Condensed Matter **31**, 095802 (2019-03-06).
[23] T. F. Chan, G. H. Golub, and R. J. Leveque, The American Statist **37**, 242 (1983).
[24] P. de Loth, P. Cassoux, J. P. Daudey, and J. P. Malrieu, J . Am. Chem. SOC **103**, 4007 (1981).
[25] M.-B. Lepetit, Recent Research Developments in Quantum Chemistr 3 (Transword Research Network, 2002) p. 143.
[26] I. Lindgren and J. Morrison, Atomic Many-Body Theory, edited by J. P. Toennies, Vol. 13 (Springer-Verlag Berlin Heidelberg New York, 1982).
[27] J. B. Goodenough, Magnetism and the chemical bond (Company, Robert E. Krieger Publishing, 1963).
[28] K. Momma and F. Izumi, J. Appl. Cryst. **44**, 1272 (2011).
[29] U. Varetto, Molekel 5.4 (2009).